Bifurcation tunneling dynamics in the water trimer

Frank N. Keutsch[a] and Richard J. Saykally[b]
Department of Chemistry, University of California at Berkeley, Berkeley, California 94720

David J. Wales[c]
University Chemical Laboratories, Lensfield Road, Cambridge CB2 1EW, United Kingdom

(Received 12 June 2002; accepted 6 August 2002)

Recent far-infrared vibration–rotation–tunneling experiments have probed intricate details of the hydrogen bond tunneling dynamics in the water trimer through excitation of intermolecular vibrational transitions to states of sequentially increasing energy. The experimentally observed bifurcation splitting in the water trimer evolves from an equally spaced quartet in the vibrational ground state to a slightly asymmetrical quartet for intermediate torsional vibrational states lying below 100 cm^{-1}. Even more asymmetric bifurcation splittings have been observed in the out-of-plane librational band of $(H_2O)_3$ near 520 cm^{-1}. These patterns may be caused by the bifurcation and flip rearrangements becoming comparable in magnitude. Alternatively, some of the data can be fitted by introducing tunneling matrix elements corresponding to multiple elementary rearrangements. Analysis of the observed bifurcation tunneling splittings of $(D_2O)_3$ confirms that the dominant bifurcation pathway includes the torsional flipping motion of the neighboring water molecules. Quantification of the bifurcation matrix elements of $(D_2O)_3$ furthermore reveals that these vary within each torsional manifold. © *2002 American Institute of Physics.*
[DOI: 10.1063/1.1509750]

I. INTRODUCTION

The study of small water clusters in the gas phase is motivated by the quest for an accurate intermolecular potential energy surface for liquid water,[1–6] and for a detailed molecular description of the associated hydrogen bond rearrangement dynamics.[7–35] Ultimately, we seek to understand quantitatively every detail of the extensive terahertz vibration–rotation–tunneling (VRT) spectra now available for various isotopomers of the dimer, trimer, tetramer, pentamer, and hexamer, in the anticipation that such a detailed understanding of these small systems will illuminate the nature of the bulk phases of water. While we are presently converging towards such a complete description of the water dimer via complete treatments of the VRT dynamics occurring on global potential surfaces, our understanding of the larger clusters is much less complete.[2–6]

Bifurcation and torsional tunneling (see Fig. 1) both result in observable splittings in VRT spectra of the water trimer.[7] Bifurcation tunneling has not been studied in as much detail as has torsional tunneling; however, it has now been observed for the water dimer through hexamer, except for the tetramer.[17] This motion is of particular interest, as it is the lowest energy pathway for breaking and making hydrogen bonds in water clusters, and correlates with the librational motions thought to effect such processes in the liquid.[14] Analysis of the bifurcation tunneling splitting has recently provided an estimate of the hydrogen bond lifetime in the water trimer; the result is remarkably similar to the predictions from models for liquid water.[14]

II. BACKGROUND: TUNNELING IN THE WATER TRIMER

The oblate symmetric top spectrum of water trimer results from vibrational averaging over large amplitude torsional motions of the unbound hydrogens on the time scale of the FIR-VRT experiment (Fig. 1). This torsional motion occurs via the facile ''flip'' process, which was first characterized for an empirical potential.[36] The first *ab initio* flipping pathway was presented by Wales,[7] while Fowler and Schaefer also characterized the corresponding transition state.[37] Wales originally identified two other degenerate rearrangement mechanisms (rearrangements between permutational isomers) for the trimer having much larger barriers, and suggested that one of them (the ''donor'' or ''bifurcation'' pathway) might be responsible for the regular quartet splittings observed experimentally at high resolution. In this mechanism, one water monomer becomes a double hydrogen bond donor in the transition state, rotating roughly about the local axis perpendicular to the monomer plane (not the C_2 axis) as shown in Fig. 1.

From the experimentally determined intensity and splitting patterns, it is possible to gain quantitative insight into the bifurcation tunneling dynamics. This insight requires a molecular symmetry group analysis and construction of the reaction graph corresponding to the ''feasible''[38] mechanisms to evaluate the contribution of different tunneling pathways to the overall tunneling in each vibrational level. The first detailed theoretical description of torsional and bifurcation tunneling in the water trimer considered various

[a]Present address: Department of Chemistry and Chemical Biology, Harvard University, Cambridge, Massachusetts 02138.
[b]Electronic mail: saykally@uclink4.berkeley.edu
[c]Electronic mail: dw34@cam.ac.uk

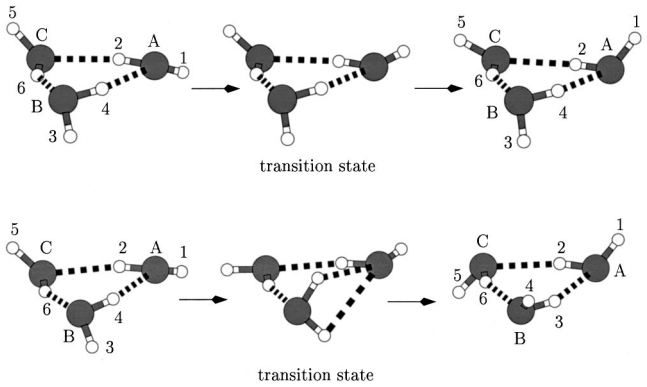

FIG. 1. Flip (top) and bifurcation (bottom) rearrangements of water trimer. The oxygen atoms are labeled *A*, *B*, and *C* and the hydrogens are numbered from one to six. For the labeled reference structure shown the corresponding generators are $(ACB)(153)(264)^*$ and $(34)^*$, respectively. The bifurcation corresponds to the majority acceptor+double flip pathway, classified as type B3.

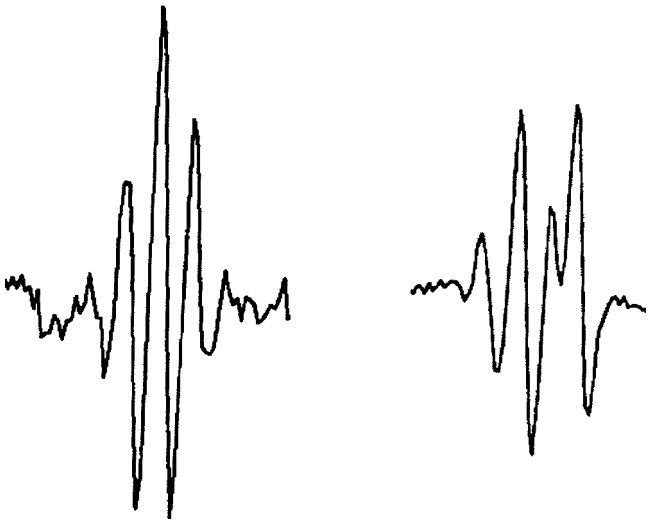

FIG. 2. The two main types of bifurcation tunneling splittings observed experimentally. The regular quartet splitting of the 28 cm^{-1} $(D_2O)_3$ band (left) exhibits a regular spacing of 0.9 MHz and intensity pattern 1:5:10:7. Such regular quartets are observed for all transitions except for $|K|=0 \leftarrow 1$. For the latter transitions "anomalous" quartets are observed (right), which have a similar but nonconstant spacing of about 0.9 MHz. The intensity pattern of the "anomalous" quartets is roughly 2:9:4:6, and the varying linewidth is caused by the overlap of multiple transitions.

tunneling pathways for both empirical and *ab initio* potentials, and applied a Hückel model to calculate the tunneling splittings.[7] Gregory and Clary presented a numerical treatment of both the torsional and bifurcation tunneling in the ground states of the trimer using the DQMC approach.[16]

The single flip mechanism (Fig. 1) links each permutational isomer to two others in sets of six, giving a secular problem from degenerate perturbation theory isomorphic to the π system of benzene[7,39] with the splitting pattern,

$$2\beta_{1f}(A_1), \quad \beta_{1f}(E_2), \quad -\beta_{1f}(E_1), \quad -2\beta_{1f}(A_2), \quad (1)$$

where β_{1f} is the tunneling matrix element for the flip. The molecular symmetry group[40] has order six and is isomorphic to C_{3h}.[41] van der Avoird *et al.* employed an alternative notation for the irreducible representations (IR's) of this group, writing the permutation-inversion generator for the flip as $\mathcal{F}=(\mathrm{ACB})(153)(264)^*$.[11] The complex characters can then be written as $\chi^{(k)}(\mathcal{F}^n)=\exp(nk\pi i/3)$ for IR's $A_1^+ \equiv A_1$, $(k=0)$, $\{A_2^-, A_3^-\} \equiv E_2$, $(k=\pm 1)$, $\{A_3^+, A_2^+\} \equiv E_1$, $(k=\pm 2)$ and $A_1^- \equiv A_2$, $(k=3)$.

There is now general agreement that the quartet splittings observed experimentally (see Fig. 2) are due to bifurcation tunneling. When both the bifurcation mechanism and the single flip are feasible, the molecular symmetry group, $G(48)$, has order 48 (Ref. 7) and is identical to the group deduced in previous work for the acetylene trimer[42] (Table I). Walsh and Wales subsequently made an extensive analysis of the bifurcation tunneling pathway, especially regarding the number of simultaneous torsional flips of neighboring water molecules, and found that the details of the path were very sensitive to the level of *ab initio* theory employed.[8] The most recent calculations of Taketsugu and Wales suggest that the pathways calculated for bifurcation pass close to a transition state for a single flip rearrangement.[43] The motion of the bifurcating water molecule is not sensitive to the level of theory used, but the number of associated flips seems to change with the basis set or the correlation energy treatment in an unpredictable way. This result is clearly due to the facile nature of the flip compared to the bifurcation, since the torsional rearrangement is a relatively small perturbation to the bifurcation path.

In the limit where the bifurcation tunneling matrix element is small compared to the torsional tunneling matrix element, Wales and Walsh found that only two different splitting patterns resulted from the six possible combinations of flips that produce a degenerate rearrangement[44] in combination with bifurcation tunneling.[10] The same molecular symmetry group,[40] $G(48)$ (Table I), applies to both cases. These splitting patterns were designated "*A*" and "*B*," each associated with three of the six possible flip combinations (Table II). van der Avoird *et al.* also considered two of the possible generators for bifurcation rearrangements, namely (ACB)(164253) and $(34)^*$, corresponding to *A*1 and *B*3 in Table II.[11] They reproduced the patterns deduced by Walsh and Wales,[10] enabling Olthof *et al.* to show that the $k=3 \leftarrow k=0$ transitions in the 41.1 cm^{-1} band of $(D_2O)_3$ follow the *B*, rather than *A*, pattern under the assumption that the tunneling matrix element is constant within each torsional manifold.[35] Although van der Avoird *et al.*[11] describe the bifurcation tunneling splittings somewhat differently from the previous work,[7,10] the results are, in fact, the same. The 48 permutational isomers that are linked by single flip and bifurcation rearrangements are split into states with degeneracies 8:16:16:8 by the flip mechanism alone, as in Eq. (1). Bifurcation tunneling splits each of these four sets of states into quartets in both the *A* and *B* patterns,[7,10,11] albeit with accidental degeneracies in the $k=\pm 1$ and $k=\pm 2$ sets (see Table III for the *B* pattern) neglecting effects of Coriolis perturbations.

Bifurcation tunneling has been observed for nearly all $(D_2O)_3$ and $(H_2O)_3$ VRT bands, however, the details of these tunneling splittings, such as the magnitude of the splitting, intensity patterns, and irregularities have never been

TABLE I. The character table for the $G(48)$ molecular symmetry group of the water trimer, including nuclear spin weights for both $(D_2O)_3$ and $(H_2O)_3$. The $\pm$ superscript indicates the parity under the E^* operation; $\epsilon = \exp(i\pi/3)$. An alternative notation for the IR's uses g and u subscripts to indicate the parity under the $(12)(34)(56)^*$ operation (Ref. 11), but we have retained the labels used in earlier work to avoid any possible confusion with the point group inversion operation.

	D_2O_3	H_2O_3	E	4 (*ACB*) (164253)	4 (*ABC*) (135246)	4 (*ABC*) (153) (264)	4 (*ABC*) (145) (236)	3 (12)	3 (12) (34)	(12) (34) (56)	E^*	4 (*ACB*) (164253)*	4 (*ABC*) (135246)*	4 (*ABC*) (153) (264)*	4 (*ABC*) (145) (236)*	3 (12)*	3 (12) (34)*	(12) (34) (56)*
A_1^+	76	1	1	1	1	1	1	1	1	1	1	1	1	1	1	1	1	1
A_1^-	76	1	1	1	1	1	1	1	1	1	−1	−1	−1	−1	−1	−1	−1	−1
A_2^+	11	11	1	−1	−1	1	1	−1	1	−1	1	−1	−1	1	1	−1	1	−1
A_2^-	11	11	1	−1	−1	1	1	−1	1	−1	−1	1	1	−1	−1	1	−1	1
E_1^+	8	8	1	ϵ	ϵ^*	$-\epsilon$	$-\epsilon^*$	−1	1	−1	1	ϵ	ϵ^*	$-\epsilon$	$-\epsilon^*$	−1	1	−1
	8	8	1	ϵ^*	ϵ	$-\epsilon^*$	$-\epsilon$	−1	1	−1	1	ϵ^*	ϵ	$-\epsilon^*$	$-\epsilon$	−1	1	−1
E_2^+	70	0	1	$-\epsilon^*$	$-\epsilon$	$-\epsilon^*$	$-\epsilon$	1	1	1	1	$-\epsilon^*$	$-\epsilon$	$-\epsilon^*$	$-\epsilon$	1	1	1
	70	0	1	$-\epsilon$	$-\epsilon^*$	$-\epsilon$	$-\epsilon^*$	1	1	1	1	$-\epsilon$	$-\epsilon^*$	$-\epsilon$	$-\epsilon^*$	1	1	1
E_1^-	8	8	1	ϵ	ϵ^*	$-\epsilon$	$-\epsilon^*$	−1	1	−1	−1	$-\epsilon$	$-\epsilon^*$	ϵ	ϵ^*	1	−1	1
	8	8	1	ϵ^*	ϵ	$-\epsilon^*$	$-\epsilon$	−1	1	−1	−1	$-\epsilon^*$	$-\epsilon$	ϵ^*	ϵ	1	−1	1
E_2^-	70	0	1	$-\epsilon^*$	$-\epsilon$	$-\epsilon^*$	$-\epsilon$	1	1	1	−1	ϵ^*	ϵ	ϵ^*	ϵ	−1	−1	−1
	70	0	1	$-\epsilon$	$-\epsilon^*$	$-\epsilon$	$-\epsilon^*$	1	1	1	−1	ϵ	ϵ^*	ϵ	ϵ^*	−1	−1	−1
T_1^+	108	3	3	0	0	0	0	1	−1	−3	3	0	0	0	0	1	−1	−3
T_2^+	54	9	3	0	0	0	0	−1	−1	3	3	0	0	0	0	−1	−1	3
T_1^-	108	3	3	0	0	0	0	1	−1	−3	−3	0	0	0	0	−1	1	3
T_2^-	54	9	3	0	0	0	0	−1	−1	3	−3	0	0	0	0	1	1	−3

TABLE II. The twelve combinations for exchanging the free and bound hydrogen on each monomer together with 0, 1, or 2 flips of neighboring monomers are listed together with the permutation–inversion generator operations. The generators are based on the labeled trimer structure depicted in Fig. 1, which is the same as in previous work (Refs. 7, 10). Monomer *A* is the maj(ority) donor, *B* the maj(ority) acceptor and *C* the min(ority) monomer. The level of theory of calculations at which each pathway was found is also shown, along with the *A*1-3 and *B*1-3 classifications used in previous work (Refs. 10, 43). Nondegenerate rearrangements (Ref. 44) link the global minimum to a "crown" structure (Refs. 10, 43).

Number	Description	Generator	
1	min+no flips	nondegenerate	
$(A2)$ $2 \equiv 6^{-1}$	min+maj donor flip	$(ABC)(136245)$	Not found
$(A1)$ $3 \equiv 10^{-1}$	min+maj acceptor flip	$(ACB)(164253)$	EPEN
			DZP/SCF
			DZP/BLYP
			aug-cc-pVDZ/MP2
			aug-cc-pVTZ/MP2
$(B1)$ 4	min+double flip	$(56)^*$	DZP+diff/SCF
			4-31G/SCF
$(A3)$ $5 \equiv 9^{-1}$	maj acceptor+no flips	$(ABC)(143625)^*$	ASP-W2
			DZP+diff/BLYP
			DZP/MP2
			6-31G**/SCF
			4-31G**/SCF
			ASP-W4
$(A2)$ $6 \equiv 2^{-1}$	maj acceptor+min flip	$(ACB)(154263)$	Not found
7	acceptor+maj donor flip	nondegenerate	
$(B3)$ 8	maj acceptor+double flip	$(34)^*$	TIP4P
$(A3)$ $9 \equiv 5^{-1}$	maj donor+no flips	$(ACB)(152634)^*$	ASP-W2
			DZP+diff/BLYP
			DZP/MP2
			6-31G**/SCF
			4-31G**/SCF
			ASP-W4
$(A1)$ $10 \equiv 3^{-1}$	maj donor+min flip	$(ABC)(135246)$	EPEN
			DZP/SCF
			DZP/BLYP
			aug-cc-pVDZ/MP2
			aug-cc-pVTZ/MP2
11	donor+acceptor flip	nondegenerate	
$(B2)$ 12	maj donor+double flip	$(12)^*$	Not found

TABLE III. General B splitting pattern for water trimer and J, $K=0$ when the only nonzero matrix elements considered are β_{1b} and β_{1f}. The two limits $|\beta_{1b}|\ll|\beta_{1f}|$ and $|\beta_{1b}|\gg|\beta_{1f}|$ are given as series expansions correct to order β_{1b}^2 and β_{1f}^2, respectively. The parameter $c^{\pm}=\sqrt{9\beta_{1f}^2\pm4\beta_{1f}\beta_{1b}+4\beta_{1b}^2}$.

$\lvert\beta_{1b}\rvert\ll\lvert\beta_{1f}\rvert$	General	$\lvert\beta_{1b}\rvert\gg\lvert\beta_{1f}\rvert$	Irrep
$2\beta_{1f}+\beta_{1b}$	$2\beta_{1f}+\beta_{1b}$	$\beta_{1b}+2\beta_{1f}$	A_1^+
$\frac{3\lvert\beta_{1f}\rvert+\beta_{1f}}{2}+\frac{\lvert\beta_{1f}\rvert\beta_{1b}}{3\beta_{1f}}+\frac{8\beta_{1b}^2}{27\lvert\beta_{1f}\rvert}$	$\frac{\beta_{1f}+c^+}{2}$	$\lvert\beta_{1b}\rvert+\frac{\beta_{1f}(\beta_{1b}+\lvert\beta_{1b}\rvert)}{2\beta_{1b}}+\frac{\beta_{1f}^2}{\lvert\beta_{1b}\rvert}$	T_1^+
$\frac{3\lvert\beta_{1f}\rvert+\beta_{1f}}{2}-\frac{\lvert\beta_{1f}\rvert\beta_{1b}}{3\beta_{1f}}+\frac{8\beta_{1b}^2}{27\lvert\beta_{1f}\rvert}$	$\frac{\beta_{1f}+c^-}{2}$	$\lvert\beta_{1b}\rvert+\frac{\beta_{1f}(\beta_{1b}-\lvert\beta_{1b}\rvert)}{2\beta_{1b}}+\frac{\beta_{1f}^2}{\lvert\beta_{1b}\rvert}$	T_2^+
$2\beta_{1f}-\beta_{1b}$	$2\beta_{1f}-\beta_{1b}$	$-\beta_{1b}+2\beta_{1f}$	A_2^+
$\beta_{1f}+\beta_{1b}$	$\beta_{1f}+\beta_{1b}$	$\beta_{1b}+\beta_{1f}$	E_1^-, T_2^-
$\frac{3\lvert\beta_{1f}\rvert-\beta_{1f}}{2}+\frac{\lvert\beta_{1f}\rvert\beta_{1b}}{3\beta_{1f}}+\frac{8\beta_{1b}^2}{27\lvert\beta_{1f}\rvert}$	$\frac{c^+-\beta_{1f}}{2}$	$\lvert\beta_{1b}\rvert-\frac{\beta_{1f}(\beta_{1b}-\lvert\beta_{1b}\rvert)}{2\beta_{1b}}+\frac{\beta_{1f}^2}{\lvert\beta_{1b}\rvert}$	T_1^-
$\frac{3\lvert\beta_{1f}\rvert-\beta_{1f}}{2}-\frac{\lvert\beta_{1f}\rvert\beta_{1b}}{3\beta_{1f}}+\frac{8\beta_{1b}^2}{27\lvert\beta_{1f}\rvert}$	$\frac{c^--\beta_{1f}}{2}$	$\lvert\beta_{1b}\rvert-\frac{\beta_{1f}(\beta_{1b}+\lvert\beta_{1b}\rvert)}{2\beta_{1b}}+\frac{\beta_{1f}^2}{\lvert\beta_{1b}\rvert}$	T_2^-
$\beta_{1f}-\beta_{1b}$	$\beta_{1f}-\beta_{1b}$	$-\beta_{1b}+\beta_{1f}$	E_2^-, T_1^-
$\beta_{1f}+\beta_{1b}$	$-\beta_{1f}+\beta_{1b}$	$\beta_{1b}-\beta_{1f}$	E_2^+, T_1^+
$-\frac{(3\lvert\beta_{1f}\rvert-\beta_{1f})}{2}+\frac{\lvert\beta_{1f}\rvert\beta_{1b}}{3\beta_{1f}}-\frac{8\beta_{1b}^2}{27\lvert\beta_{1f}\rvert}$	$\frac{\beta_{1f}-c^-}{2}$	$-\lvert\beta_{1b}\rvert+\frac{\beta_{1f}(\beta_{1b}+\lvert\beta_{1b}\rvert)}{2\beta_{1b}}-\frac{\beta_{1f}^2}{\lvert\beta_{1b}\rvert}$	T_2^+
$-\frac{(3\lvert\beta_{1f}\rvert-\beta_{1f})}{2}-\frac{\lvert\beta_{1f}\rvert\beta_{1b}}{3\beta_{1f}}-\frac{8\beta_{1b}^2}{27\lvert\beta_{1f}\rvert}$	$\frac{\beta_{1f}-c^+}{2}$	$-\lvert\beta_{1b}\rvert+\frac{\beta_{1f}(\beta_{1b}-\lvert\beta_{1b}\rvert)}{2\beta_{1b}}-\frac{\beta_{1f}^2}{\lvert\beta_{1b}\rvert}$	T_1^+
$-\beta_{1f}-\beta_{1b}$	$-\beta_{1f}-\beta_{1b}$	$-\beta_{1b}-\beta_{1f}$	E_1^+, T_2^+
$-2\beta_{1f}+\beta_{1b}$	$-2\beta_{1f}+\beta_{1b}$	$\beta_{1b}-2\beta_{1f}$	A_2^-
$-\frac{(3\lvert\beta_{1f}\rvert+\beta_{1f})}{2}+\frac{\lvert\beta_{1f}\rvert\beta_{1b}}{3\beta_{1f}}-\frac{8\beta_{1b}^2}{27\lvert\beta_{1f}\rvert}$	$-\frac{(\beta_{1f}+c^-)}{2}$	$-\lvert\beta_{1b}\rvert-\frac{\beta_{1f}(\beta_{1b}-\lvert\beta_{1b}\rvert)}{2\beta_{1b}}-\frac{\beta_{1f}^2}{\lvert\beta_{1b}\rvert}$	T_2^-
$-\frac{(3\lvert\beta_{1f}\rvert+\beta_{1f})}{2}-\frac{\lvert\beta_{1f}\rvert\beta_{1b}}{3\beta_{1f}}-\frac{8\beta_{1b}^2}{27\lvert\beta_{1f}\rvert}$	$-\frac{(\beta_{1f}+c^+)}{2}$	$-\lvert\beta_{1b}\rvert-\frac{\beta_{1f}(\beta_{1b}+\lvert\beta_{1b}\rvert)}{2\beta_{1b}}-\frac{\beta_{1f}^2}{\lvert\beta_{1b}\rvert}$	T_1^-
$-2\beta_{1f}-\beta_{1b}$	$-2\beta_{1f}-\beta_{1b}$	$-\beta_{1b}-2\beta_{1f}$	A_1^-

reported or discussed in depth for all observed bands. Therefore, a brief review of the experimental results will follow. Table IV summarizes the bifurcation splittings of all the observed $(D_2O)_3$ and $(H_2O)_3$ vibrational bands, and Fig. 2 shows typical examples of the experimentally observed bifurcation splittings. Table IV demonstrates that two cases for the ordering of the quartets are observed. The different orderings arise because the experimental splittings correspond to the difference of the bifurcation tunneling splitting in the lower and upper levels, and the sign of the bifurcation tunneling matrix elements can be either positive or negative.

The observed bifurcation splittings can be divided into two different types: most of the observed bifurcation splittings consist of equally spaced quartets with an intensity pattern of ~7:11:5:1 in $(D_2O)_3$ (see Fig. 2 left) and 1:3:9:11 for $K=3m$ and 0:3:9:8 for $K\neq3m$ in $(H_2O)_3$. These quartets will henceforth be referred to as ''regular'' quartets. ''Anomalous'' quartets with intensity patterns distinct from the ''regular'' quartets and slightly unequal spacing (see Fig. 2 right) are only observed for some of the transitions involving $K=0$ (K is the quantum number for the projection of the overall rotation onto the pseudo-threefold axis of the water trimer). Both sets of ''quartets'' will be discussed in detail. Lastly, there are some additional splitting of bifurcation tunneling components that are J-dependent, arising from Coriolis coupling. J is the quantum number for the total angular momentum. The splitting of the quartets varies between 1 and 10 MHz and between 40 and >40 000 MHz for $(D_2O)_3$ and $(H_2O)_3$, respectively. The splitting is larger for $(H_2O)_3$ because of the smaller mass, and, furthermore, the 520 cm^{-1} librational band has a much higher frequency and, thus higher internal energy than any $(D_2O)_3$ band.

Although the observed bifurcation splittings generally increase with the energy of the vibrational band for both $(D_2O)_3$ and $(H_2O)_3$, we note that these splittings depend on the sign of the bifurcation matrix element in the upper and lower rovibrational state, and thus may not follow a clear trend. Furthermore, no regular quartets were observed in the 142.8 cm^{-1} band of $(D_2O)_3$, the highest energy $(D_2O)_3$ VRT band observed to date. Thus, it follows that the bifurcation splitting is too small to be determined experimentally (<1 MHz) and that the magnitude of the splitting does not change significantly between the upper and lower vibrational states.

Table IV shows that anomalous quartets are observed for $K=0$ rotational states of all $(D_2O)_3$ bands involving $k=\pm1$ and $k=\pm2$ levels, which will be discussed later. All states with $|K|>0$, except for the $K=2$ states of the 19.5 cm^{-1} band, exhibit regular quartets. The J-dependent splitting of the $K=2$ states of the 19.5 cm^{-1} $(D_2O)_3$ band was only observed for high J values, and results from Coriolis perturbations that appear beyond second order. The analysis of the anomalous quartets of $(D_2O)_3$ provides valuable insight into the details of the bifurcation tunneling dynamics.[35] Specifically, the anomalous quartets of the 28 and 98 cm^{-1} $(D_2O)_3$ bands will be used in our analysis, as these are the only ones that have adequate intensity and have been sufficiently well characterized.

In the degenerate $k=\pm1$ and $k=\pm2$ states of $(H_2O)_3$ such a clear distinction between anomalous and regular bi-

TABLE IV. All observed $(D_2O)_3$ and $(H_2O)_3$ vibrational transitions are shown with the torsional k assignment, vibrational band origin, ν (cm^{-1}), and the approximate intensity pattern of the anomalous bifurcation splittings. The regular quartets are equally spaced and the splittings listed are for the order A_1^+, T_1^+, T_2^+, A_2^+, thus, a negative value indicates that A_1^+ is the highest frequency component of the quartet. The K values for which "anomalous" bifurcation splittings are observed are shown, and J-dependent splittings proportional to $J(J+1)$ are indicated.

Assignment $k''\leftarrow k'$	ν	Regular quartet splitting (MHz)	Anomalous splitting	
			Transitions	Intensities
		$(D_2O)_3$		
$\pm 2^0 \leftarrow \mp 1^0$ [a]	19.5	<1	$K=2\leftarrow 2$, $J(J+1)$	2.5:1:1:2.5
			$K=0\leftarrow 0$ 2 MHz	1:2
$\pm 2^0 \leftarrow 0^0$ [b]	28.0	-0.9	$K=0\leftarrow 1$ $\sim$0.9 MHz	2:9:4:6
$3^0 \leftarrow 0^0$ [b]	41.1	-1.5[e]	Not observed	
$3^1 \leftarrow \pm 1^0$ [b]	81.8	2.7[b] 5[f]	$K=1\leftarrow 0$ $\sim$2.7 MHz[b]	5:3:5:2
$\pm 2^1 \leftarrow \mp 1^0$ [b]	89.6	6[g]	UK	
$\pm 2^1 \leftarrow 0^0$ [b]	98.0	5[f]	$K=0\leftarrow 1$ $\sim$5 MHz[h]	8:2:4:3
$\pm 2^{trans} \leftarrow \pm 0^0$ [c]	142.8	<1	$K=0\leftarrow 1$ $\sim$10 MHz	1:1:1
		$(H_2O)_3$		
$\pm 2^0 \leftarrow \mp 1^0$ [d]	42.9	39	shift of T states	
$\pm 2^0 \leftarrow 0^0$ [d]	65.6	-255	shift of T states	
$3^0 \leftarrow 0^0$ [d]	87.1	-289[f]	T states $K=1\leftarrow 1$, $J(J+1)$	1:1
Libration	$\sim$520	$>40\,000$	T states of 523.9 cm^{-1} band $K=1\leftarrow 1$, $J(J+1)$	1:1

[a]Reference 22.
[b]Reference 26.
[c]Reference 24.
[d]Reference 23.
[e]Reference 55.
[f]Reference 56.
[g]Reference 41.
[h]Reference 35.

TABLE V. The torsional and bifurcation tunneling levels for $K=0$ and $K=1$ are shown with both the A and B pattern contributions from bifurcation tunneling. β_A, β_B refer to the bifurcation matrix elements for the A and B patterns, respectively. No assumption about the details of the tunneling pathways or simultaneous contributions of different pathways following either the A or B pattern is made. For $K=0$ there are no Coriolis effects. For $K>0$, $k-K$ labels cannot be rigorously assigned for the T states if Coriolis effects are included. The $K=1$ T states of $k=0$ and 3 are split via Coriolis coupling with the $K=0$ T states of $k=\pm 1$, ± 2, which is not shown. Coriolis coupling would also split the two sets of bifurcation components of the $k-K=0$ states of $k=\pm 1$, as well as the $k-K=3$ states of $k=\pm 2$. However, the T states of $k-K=\pm 2$, $k=\pm 1$ and $k-K=\pm 1$, $k=\pm 2$ would not be split by Coriolis coupling as they are not degenerate. Therefore, anomalous quartets can only be observed for transitions involving $K=0$ and the $k=\pm 1$, $k=\pm 2$ torsional levels. The notation $2A_1^+$ indicates that two levels of A_1^+ symmetry exist. These accidental degeneracies would be split by Coriolis interactions.

	$K=0$		$K=\pm 1$	
	$k-K=0$		$k-K=\pm 1$	
$k=0$	A_1^+	$2\beta_A+\beta_B$	E_2^-	$2\beta_A+\beta_B$
	T_1^+	$\frac{2}{3}\beta_A+\frac{1}{3}\beta_B$	$2T_1^-$	$\frac{2}{3}\beta_A+\frac{1}{3}\beta_B$
	T_2^+	$-\frac{2}{3}\beta_A-\frac{1}{3}\beta_B$	$2T_2^-$	$-\frac{2}{3}\beta_A-\frac{1}{3}\beta_B$
	A_2^+	$-2\beta_A-\beta_B$	E_1^-	$-2\beta_A-\beta_B$
	$k-K=\pm 1$		$k-K=0$	$k-K=\pm 2$
$k=\pm 1$	E_2^-	$-\beta_A-\beta_B$	$2A_1^+$ $-\beta_A-\beta_B$	E_2^+ $-\beta_A-\beta_B$
	T_1^-	$\beta_A-\beta_B$	$2T_1^+$ $-\frac{1}{3}\beta_A-\frac{1}{3}\beta_B$	$2T_1^+$ $-\frac{1}{3}\beta_A-\frac{1}{3}\beta_B$
	T_1^-	$-\frac{5}{3}\beta_A+\frac{1}{3}\beta_B$		
	T_2^-	$\frac{5}{3}\beta_A-\frac{1}{3}\beta_B$	$2T_2^+$ $\frac{1}{3}\beta_A+\frac{1}{3}\beta_B$	$2T_2^+$ $\frac{1}{3}\beta_A+\frac{1}{3}\beta_B$
	T_2^-	$-\beta_A+\beta_B$		
	E_1^-	$\beta_A+\beta_B$	$2A_2^+$ $\beta_A+\beta_B$	E_1^+ $\beta_A+\beta_B$
	$k-K=\pm 2$		$k-K=\pm 1$	$k-K=3$
$k=\pm 2$	E_2^+	$-\beta_A+\beta_B$	E_2^- $-\beta_A+\beta_B$	$2A_1^-$ $-\beta_A+\beta_B$
	T_1^+	$\beta_A+\beta_B$	$2T_1^-$ $-\frac{1}{3}\beta_A+\frac{1}{3}\beta_B$	$2T_1^-$ $-\frac{1}{3}\beta_A+\frac{1}{3}\beta_B$
	T_1^+	$-\frac{5}{3}\beta_A-\frac{1}{3}\beta_B$		
	T_2^+	$\frac{5}{3}\beta_A+\frac{1}{3}\beta_B$	$2T_2^-$ $\frac{1}{3}\beta_A-\frac{1}{3}\beta_B$	$2T_2^-$ $\frac{1}{3}\beta_A-\frac{1}{3}\beta_B$
	T_2^+	$-\beta_A-\beta_B$		
	E_1^+	$\beta_A-\beta_B$	E_1^- $\beta_A-\beta_B$	$2A_2^-$ $\beta_A-\beta_B$
	$k-K=3$		$k-K=\pm 2$	
$k=3$	A_1^-	$2\beta_A-\beta_B$	E_2^+ $2\beta_A-\beta_B$	
	T_1^-	$\frac{2}{3}\beta_A-\frac{1}{3}\beta_B$	$2T_1^+$ $\frac{2}{3}\beta_A-\frac{1}{3}\beta_B$	
	T_2^-	$-\frac{2}{3}\beta_A+\frac{1}{3}\beta_B$	$2T_2^+$ $-\frac{2}{3}\beta_A+\frac{1}{3}\beta_B$	
	A_2^-	$-2\beta_A+\beta_B$	E_1^+ $-2\beta_A+\beta_B$	

furcation tunneling quartets is not possible, because the bifurcation splittings are comparable to the shifts and splittings caused by the Coriolis perturbation and the spacing of the rotational levels.

From the analysis of the 41 and 98 cm^{-1} $(D_2O)_3$ bands, and the 87.1 cm^{-1} $(H_2O)_3$ band, Olthof *et al.* concluded that the bifurcation tunneling matrix element $\beta_{1b}(n^0)$ is -1.1 MHz for $k=n^0$ (lowest torsional manifold, $n=0$, ± 1, ± 2, 3) and $\beta_{1b}(n^1)=-7.5$ MHz for $k=n^1$ (first excited torsional manifold) in $(D_2O)_3$, and $\beta_{1b}(n^0)=-217$ MHz for $k=n^0$ in $(H_2O)_3$.[35] The first excited torsional manifold corresponds to the symmetry adapted combinations of the 48 localized first excited states.

If β_{1b}, the matrix element corresponding to an elementary bifurcation, is constant within the first torsional manifold, then considering all the symmetry allowed transitions within this manifold, we find that the observed spacing between the regular quartet components should be $-\frac{4}{3}\beta_{1b}$ ($3\leftarrow 0$), $\frac{4}{3}\beta_{1b}$ ($\pm 2\leftarrow\pm 1$) or zero ($3\leftarrow\pm 1$ and $\pm 2\leftarrow 0$) for the B pattern (see Tables V and VI).[10] The results in Table IV, which include additional bands observed after the analysis of Olthof *et al.*, demonstrate that the premise of constant bifurcation matrix elements within each torsional manifold is not realized and therefore a reanalysis of the tunneling dynamics is necessary.

Recently, Brown *et al.* presented a quantitative characterization of the torsional energy levels of $(H_2O)_3$, which includes a fit of all the bifurcation tunneling components.[23] Although Brown *et al.* were able to fit all the $(H_2O)_3$ bands below 100 cm^{-1}, the observed shifts of the T states with respect to the A states had to be fitted to an empirical expression without a theoretical explanation. An $(H_2O)_3$ librational band at about 520 cm^{-1} has also been observed with a very large (>1 cm^{-1}) and irregularly spaced splitting.[25] These results indicate that further development of the theory of tunneling in the water trimer is in order.

van der Avoird *et al.* showed that there is no first-order Coriolis splitting in water trimer, but in second-order, new *J*-dependent effects occur, where *J* is the quantum number for overall rotation.[11,22,23] The Coriolis interaction lifts the accidental degeneracy (time reversal) between the $k=\pm 1$ levels (and the $k=\pm 2$ levels) and, thus, introduces further splittings. When the *J* quantum number for total angular momentum is nonzero, significant Coriolis effects can occur, including splittings that result from coupling between Coriolis and bifurcation tunneling effects, and the resulting spectrum becomes quite complicated. The results also depend on *K*. The splitting of $K=0$ states arises simply from bifurcation tunneling and is *J*-independent, resulting in a quartet of states for each of $k=0$, $k=\pm 1$, $k=\pm 2$, and $k=3$ (see Tables III and V).

In vibrational transitions involving only $k=0$ and $k=3$ levels, regular quartets are observed for all *K* states, except for $K=1$ states in $(H_2O)_3$, as explained in the following paragraph. The $K=0$ bifurcation quartets in the $k=\pm 1$ and $k=\pm 2$ states include accidental degeneracies, such as E_1^-/T_2^- and E_2^-/T_1^- for $k=\pm 1$ (see Tables III and V). The splitting pattern in these quartets is different for the A and B

TABLE VI. The selection rule for water trimer vibration rotation tunneling transitions is $\Delta K-\Delta k=6m+3$ for integer *m* (Ref. 23). The allowed transitions and spin weights are shown for $K=0$ and 1. β_i' and β_i'' correspond to the bifurcation matrix elements of the upper and lower level, respectively, and $\Delta\beta_i=\beta_i'-\beta_i''$. Regular quartets are observed for all transitions except those involving $K=0$ with $k=\pm 1,\pm 2$. If the *B* pattern is dominant and β_B is constant within each manifold the regular quartet splittings are either $\pm\frac{4}{3}\beta_B$ or zero, but the observed tunneling splittings from Table IV demonstrate that this cannot be the case. Hence the magnitude of β_B depends on the torsional energy level. There are ten possible $k=\pm 2\leftarrow\pm 1$, $K=0$ transitions allowed. However, the intensity of half of the *T*-state transitions labeled with a star has been determined to be zero (Ref. 11) resulting in the observation of only six transitions. Low intensities of the 81.8 cm^{-1} $k=\pm 2^1\leftarrow\pm 1^0$ torsional hot band have precluded determination of the $K=0$ tunneling splittings in this case. In the 19.5 cm^{-1} $k=\pm 2^1\leftarrow\pm 1^0$ torsional hot band two broadened transitions spaced by about 2 MHz with unequal intensity were observed. The results shown here are only rigorously correct for $(D_2O)_3$. In $(H_2O)_3$ the *T*-state splitting of $k=\pm 1,\pm 2$ does not vanish for $K>0$, although it is dramatically reduced.

Transition $k=3\leftarrow 0$	$K=0$ $\lvert k-K\rvert=3\leftarrow 0$	Observed splitting $k=3^0\leftarrow 0^0$: -1.5 MHz
$A_1^-\leftarrow A_1^+(76)$	$[2\beta_A'-\beta_B'-(2\beta_A''+\beta_B'')]$	
$T_1^-\leftarrow T_1^+(108)$	$\frac{1}{3}[2\beta_A'-\beta_B'-(2\beta_A''+\beta_B'')]$	$\frac{2}{3}[2\Delta\beta_A-\beta_B'-\beta_B'']$
$T_2^-\leftarrow T_2^+(54)$	$-\frac{1}{3}[2\beta_A'-\beta_B'-(2\beta_A''+\beta_B'')]$	$\frac{2}{3}[2\Delta\beta_A-\beta_B'-\beta_B'']$
$A_2^-\leftarrow A_2^+(11)$	$-[2\beta_A'-\beta_B'-(2\beta_A''+\beta_B'')]$	$\frac{2}{3}[2\Delta\beta_A-\beta_B'-\beta_B'']$
	$K=0$	
$k=\mp 2\leftarrow\pm 1$	$\lvert k-K\rvert=2\leftarrow 1$	$(\mp 2^0\leftarrow\pm 1^0)$: 2 MHz
$E_2^+\leftarrow E_2^-(70/70)$	$-\beta_A'+\beta_B'+\beta_A''+\beta_B''$	
$T_1^+\leftarrow T_1^-(108)^*$	$\beta_A'+\beta_B'-(\beta_A''-\beta_B'')$	
$T_1^+\leftarrow T_1^-(108)^*$	$\beta_A'+\beta_B'+\frac{5}{3}\beta_A''-\frac{1}{3}\beta_B''$	
$T_1^+\leftarrow T_1^-(108)^*$	$-\frac{5}{3}\beta_A'-\frac{1}{3}\beta_B'-(\beta_A''-\beta_B'')$	
$T_1^+\leftarrow T_1^-(108)^*$	$-\frac{5}{3}\beta_A'-\frac{1}{3}\beta_B'+\frac{5}{3}\beta_A''-\frac{1}{3}\beta_B''$	
$T_2^+\leftarrow T_2^-(54)^*$	$\frac{5}{3}\beta_A'+\frac{1}{3}\beta_B'-\frac{5}{3}\beta_A''+\frac{1}{3}\beta_B''$	
$T_2^+\leftarrow T_2^-(54)^*$	$\frac{5}{3}\beta_A'+\frac{1}{3}\beta_B'+\beta_A''-\beta_B''$	
$T_2^+\leftarrow T_2^-(54)^*$	$-\beta_A'-\beta_B'-\frac{5}{3}\beta_A''+\frac{1}{3}\beta_B''$	
$T_2^+\leftarrow T_2^-(54)^*$	$-\beta_A'-\beta_B'+\beta_A''-\beta_B''$	
$E_1^+\leftarrow E_1^-(8/8)$	$\beta_A'-\beta_B'-\beta_A''-\beta_B''$	
	$K=0\leftarrow 1$	$(\pm 2^0\leftarrow 0^0)$: ~ -0.9 MHz
$k=\pm 2\leftarrow 0$	$k-K=2\leftarrow -1$	$(\pm 2^1\leftarrow 0^0)$: ~ 5 MHz
$E_2^+\leftarrow E_2^-(70/70)$	$-\beta_A'+\beta_B'-(2\beta_A''+\beta_B'')$	
$T_1^+\leftarrow T_1^-(108)$	$\beta_A'+\beta_B'-\frac{1}{3}(2\beta_A''+\beta_B'')$	$-2\beta_A'-\frac{2}{3}(2\beta_A''+\beta_B'')$
$T_1^+\leftarrow T_1^-(108)$	$-\frac{5}{3}\beta_A'-\frac{1}{3}\beta_B'-\frac{1}{3}(2\beta_A''+\beta_B'')$	$\frac{8}{3}\beta_A'+\frac{4}{3}\beta_B'$
$T_2^+\leftarrow T_2^-(54)$	$\frac{5}{3}\beta_A'+\frac{1}{3}\beta_B'+\frac{1}{3}(2\beta_A''+\beta_B'')$	$-\frac{10}{3}\beta_A'-\frac{2}{3}\beta_b'-\frac{2}{3}(2\beta_A''+\beta_B'')$
$T_2^+\leftarrow T_2^-(54)$	$-\beta_A'-\beta_B'+\frac{1}{3}(2\beta_A''+\beta_B'')$	$\frac{8}{3}\beta_A'+\frac{4}{3}\beta_B'$
$E_1^+\leftarrow E_1^-(8/8)$	$\beta_A'-\beta_B'+(2\beta_A''+\beta_B'')$	$-2\beta_A'-\frac{2}{3}(2\beta_A''+\beta_B'')$
	$K=1\leftarrow 0$	
$k=3\leftarrow\pm 1$	$k-K=2\leftarrow -1$	
$E_2^+\leftarrow E_2^-(70/70)$	$2\beta_A'-\beta_B'+(\beta_A''+\beta_B'')$	
$T_1^+\leftarrow T_1^-(108)$	$\frac{2}{3}\beta_A'-\frac{1}{3}\beta_B'-(\beta_A''-\beta_B'')$	$\frac{2}{3}(2\beta_A'-\beta_B')+2\beta_A''$
$T_1^+\leftarrow T_1^-(108)$	$\frac{2}{3}\beta_A'-\frac{1}{3}\beta_B'+(\frac{5}{3}\beta_A''-\frac{1}{3}\beta_B'')$	$-\frac{8}{3}\beta_A''+\frac{4}{3}\beta_B''$
$T_2^+\leftarrow T_2^-(54)$	$-\frac{2}{3}\beta_A'+\frac{1}{3}\beta_B'-(\frac{5}{3}\beta_A''-\frac{1}{3}\beta_B'')$	$\frac{2}{3}(2\beta_A'-\beta_B')+\frac{10}{3}\beta_A''-\frac{2}{3}\beta_B''$
$T_2^+\leftarrow T_2^-(54)$	$-\frac{2}{3}\beta_A'+\frac{1}{3}\beta_B'+(\beta_A''-\beta_B'')$	$-\frac{8}{3}\beta_A''+\frac{4}{3}\beta_B''$
$E_1^+\leftarrow E_1^-(8/8)$	$-2\beta_A'+\beta_B'-(\beta_A''+\beta_B'')$	$\frac{2}{3}(2\beta_A'-\beta_B')+2\beta_A''$

TABLE VI. (*Continued*.)

Transition	$K=1$	Observed splitting
$k=3\leftarrow 0$	$\lvert k-K\rvert=2\leftarrow 1$	$k=3^0\leftarrow 0^0$: -1.5 MHz
$E_2^+\leftarrow E_2^-(70/70)$	$[2\beta'_A-\beta'_B-(2\beta''_A+\beta''_B)]$	
$2T_1^+\leftarrow T_1^-(108/108)$	$\frac{1}{3}[2\beta'_A-\beta'_B-(2\beta''_A+\beta''_B)]$	$\frac{2}{3}[2\Delta\beta_A-\beta'_B-\beta''_B]$
$2T_2^+\leftarrow T_2^-(54/54)$	$-\frac{1}{3}[2\beta'_A-\beta'_B-(2\beta''_A+\beta''_B)]$	$\frac{2}{3}[2\Delta\beta_A-\beta'_B-\beta''_B]$
$E_1^+\leftarrow E_1^-(8/8)$	$-[2\beta'_A-\beta'_B-(2\beta''_A+\beta''_B)]$	$\frac{2}{3}[2\Delta\beta_A-\beta'_B-\beta''_B]$
	$K=1$	$(\mp 2^0\leftarrow\pm 1^0)<1$ MHz
$k=\mp 2\leftarrow\pm 1$	$k-K=\mp 1\leftarrow\pm 2$	$(\mp 2^1\leftarrow\pm 1^0)$: 6 MHz
$E_2^-\leftarrow E_2^+(70/70)$	$-[\beta'_A-\beta'_B-(\beta''_A+\beta''_B)]$	
$2T_1^-\leftarrow T_1^+(108/108)$	$-\frac{1}{3}[\beta'_A-\beta'_B-(\beta''_A+\beta''_B)]$	$-\frac{2}{3}[\Delta\beta_A-\beta'_B-\beta''_B]$
$2T_2^-\leftarrow T_2^+(54/54)$	$\frac{1}{3}[\beta'_A-\beta'_B-(\beta''_A+\beta''_B)]$	$-\frac{2}{3}[\Delta\beta_A-\beta'_B-\beta''_B]$
$E_1^-\leftarrow E_1^+(8/8)$	$\beta'_A-\beta'_B-(\beta''_A+\beta''_B)$	$-\frac{2}{3}[\Delta\beta_A-\beta'_B-\beta''_B]$
	$\lvert k-K\rvert=3\leftarrow 0$	
$2A_1^-\leftarrow A_1^+(76/76)$	$-[\beta'_A-\beta'_B-(\beta''_A+\beta''_B)]$	
$2T_1^-\leftarrow T_1^+(108/108)$	$-\frac{1}{3}[\beta'_A-\beta'_B-(\beta''_A+\beta''_B)]$	$-\frac{2}{3}[\Delta\beta_A-\beta'_B-\beta''_B]$
$2T_2^-\leftarrow T_2^+(54/54)$	$\frac{1}{3}[\beta'_A-\beta'_B-(\beta''_A+\beta''_B)]$	$-\frac{2}{3}[\Delta\beta_A-\beta'_B-\beta''_B]$
$2A_2^-\leftarrow A_2^+(11/11)$	$\beta'_A-\beta'_B-(\beta''_A+\beta''_B)$	$-\frac{2}{3}[\Delta\beta_A-\beta'_B-\beta''_B]$
	$K=1\leftarrow 0$	$(\pm 2^0\leftarrow 0^0)$: -0.9 MHz
$k=\pm 2\leftarrow 0$	$k-K=3\leftarrow 0$	$(\pm 2^1\leftarrow 0^0)$: 5 MHz
$A_1^-\leftarrow A_1^+(76)$	$-\beta'_A+\beta'_B-(2\beta''_A+\beta''_B)$	
$T_1^-\leftarrow T_1^+(108)$	$-\frac{1}{3}[\beta'_A-\beta'_B+(2\beta''_A+\beta''_B)]$	$-\frac{2}{3}[\beta'_A+2\beta''_A-\Delta\beta_B)]$
$T_2^-\leftarrow T_2^+(54)$	$\frac{1}{3}[\beta'_A-\beta'_B+(2\beta''_A+\beta''_B)]$	$-\frac{2}{3}[\beta'_A+2\beta''_A-\Delta\beta_B)]$
$A_2^-\leftarrow A_2^+(11)$	$[\beta'_A-\beta'_B+(2\beta''_A+\beta''_B)]$	$-\frac{2}{3}[\beta'_A+2\beta''_A-\Delta\beta_B]$
	$K=0\leftarrow 1$	
$k=3\leftarrow\pm 1$	$k-K=3\leftarrow 0$	$(3^0\leftarrow 0^0)$: 2.7/5 MHz
$A_1^-\leftarrow A_1^+(76)$	$(2\beta'_A-\beta'_B)+(\beta''_A+\beta''_B)$	
$T_1^-\leftarrow T_1^+(108)$	$\frac{1}{3}[(2\beta'_A-\beta'_B)+(\beta''_A+\beta''_B)]$	$\frac{2}{3}[2\beta'_A+\beta''_A-\Delta\beta_B]$
$T_2^-\leftarrow T_2^+(54)$	$\frac{1}{3}[(-2\beta'_A+\beta'_B)-(\beta''_A+\beta''_B)]$	$\frac{2}{3}[2\beta'_A+\beta''_A-\Delta\beta_B]$
$A_2^-\leftarrow A_2^+(11)$	$(-2\beta'_A+\beta'_B)-(\beta''_A+\beta''_B)$	$\frac{2}{3}[2\beta'_A+\beta''_A-\Delta\beta_B]$

cases: the A pattern quartets for $k=\pm 1$ and $k=\pm 2$ have symmetrical but unequal spacings, whereas the spacings are all the same throughout the B pattern.[10] Of course, the observed transitions consist of energy differences between levels. For example, in a $k=\pm 2\leftarrow 0$, $K=0\leftarrow 1$ transition the $k=0$ T_1^- and T_2^- states have allowed transitions to two T_1^+ and two T_2^+ states, respectively. There are also two allowed transitions to the E levels of $k=\pm 2$ ($E_2^+\leftarrow E_2^-$ and $E_1^+\leftarrow E_1^-$) giving six transitions altogether (see Table VI). In practice, overlapping signals as well as weak intensities for some of the transitions produce a complex pattern. The experimental results frequently appear as ''anomalous'' quartets (distinct from the ''regular'' bifurcation quartets) with slightly unequal spacing and distinct intensity patterns. These ''anomalous'' transitions are particularly important, as they provide a discrimination between the A and B patterns.

All states with $k=\pm 1$ and $k=\pm 2$ exhibit a splitting proportional to K due to second- and higher-order Coriolis perturbations, and the results resemble the effect of a first-order Coriolis interaction. This splitting lifts the degeneracy of certain $k=\pm 1$ and $k=\pm 2$ states.[22] Table V shows the resulting bifurcation splitting patterns, without the shifts and splittings introduced by the Coriolis interaction, which occur only for $K>0$. In the case of the $k=\pm 1$, $K=\pm 1$ states the Coriolis interaction splits the $k-K=\pm 2$ and $k-K=0$ states. Table V shows that for $k-K=0$ there are two sets of four bifurcation components, and these two sets are also split by the Coriolis interaction so that no accidental degeneracies remain and there is no interaction between the two T_1^+ and two T_2^+ states. For each of the two sets regular quartets are observed. The $k-K=\pm 2$ states also contain T states that are accidentally degenerate. However, the Coriolis interaction between these states is so small that it does not result in an observable splitting in $(D_2O)_3$. In $(H_2O)_3$ the splitting of such T states by Coriolis interaction and bifurcation tunneling is a complicated function of J and K for $\lvert K\rvert>0$, and decreases with K. The $K=\pm 1$ states with $k=0$ and 3 additionally exhibit a small J-dependent splitting of the T states

TABLE VII. Matrix elements considered for the tunneling problem in water trimer. The description in terms of elementary flip and bifurcation paths and the permutation–inversion generator are given in each case. The generators correspond to the labeling scheme of Fig. 1.

Matrix element	Description	PI generator
β_{1f}	flip	$(ACB)(153)(264)^*$
β_{1f}	inverse flip	$(ABC)(135)(246)^*$
β_{2f}	double flip	$(ABC)(135)(246)$
β_{2f}	inverse double flip	$(ACB)(153)(264)$
β_{3f}	triple flip	E^*
β_{1b}	bifurcation	$(34)^*$
β_{1f1b}	bifurcation then flip	$(ACB)(153264)$
β_{1f1b}	inverse flip then bifurcation	$(ABC)(146235)$
β'_{1f1b}	flip then bifurcation	$(ACB)(154263)$
β'_{1f1b}	bifurcation then inverse flip	$(ABC)(136245)$
β_{2f1b}	flip then bifurcation then inverse flip	$(56)^*$
β'_{2f1b}	inverse flip then bifurcation then flip	$(12)^*$
β''_{2f1b}	bifurcation then double flip	$(ABC)(136245)^*$
β''_{2f1b}	double inverse flip then bifurcation	$(ACB)(145263)^*$
β'''_{2f1b}	double flip then bifurcation	$(ABC)(146235)^*$
β'''_{2f1b}	bifurcation then inverse double flip	$(ACB)(153264)^*$

through Coriolis coupling to the $K=0$ T states of the $k=\pm 1$ and $k=\pm 2$ levels, respectively. This perturbation produces splittings that are proportional to $J(J+1)$, and the effects are only observable in $(H_2O)_3$.[11]

III. TUNNELING SPLITTING PATTERNS

Ideally, one would like to solve the 21-dimensional quantum nuclear dynamics problem as a function of the rotational quantum numbers,[44] but this calculation lies beyond current computational capabilities. Numerical treatments[29–31,45–52] have certainly proved useful, but including the coupling of torsional and bifurcation motion, and inter- and intramolecular degrees of freedom in excited states, remains prohibitive. Here we adopt a much simpler approach, based only on analysis of the reaction graph describing the connections between minima when particular hydrogen bond rearrangements are considered "feasible."[38]

Each feasible mechanism can be associated with a tunneling matrix element, β, (Table VII) and applying degenerate perturbation theory to the localized wave functions corresponding to different permutational isomers results in a 48×48 secular determinant. If there are only a few feasible pathways, then the spectrum of tunneling energy levels can often be represented analytically in terms of the β's. Such solutions have been presented in previous work for the limit in which the bifurcation matrix element, β_{1b}, is much smaller in magnitude than that for the flip rearrangement, β_{1f}.[7,10] In the present treatment, we give analytical expressions for the energies of the tunneling states that are valid for matrix elements of arbitrary magnitude. The limit $|\beta_{1b}| \ll |\beta_{1f}|$ is correctly reproduced, and is given in Table III together with the general form and the alternative limit $|\beta_{1b}| \gg |\beta_{1f}|$, as well as the symmetry classification of the levels in $G(48)$. We have also derived analytic expressions that include the contributions from additional pathways composed of multiple elementary flip and bifurcation rearrangements (Table VIII); the limit for small $|\beta_{1b}|$ and $|\beta_{1f1b}|$ is given in Table IX. Hence we have extended the previous Hückel-type treatment to include the interference between wave functions of nonadjacent permutational isomers. Bunker and co-workers have shown that such terms are important in other systems.[53,54]

It seems unlikely that the higher energy "crown" minimum perturbs the observed spectrum significantly.[10] We therefore consider participation of different tunneling pathways and the breakdown of the $|\beta_{1b}| \ll |\beta_{1f}|$ limit to seek an explanation for experimentally observed quartets without constant spacings, such as those reported by Brown *et al.*[23] and Keutsch *et al.*[25]

In the next section we verify that the bifurcation splitting follows the B pattern,[10] and analyze the effect of multiple tunneling pathways and the breakdown of the $|\beta_{1b}| \ll |\beta_{1f}|$ limit in this case. Matrix elements for rearrangements corresponding to combinations of n flips and m bifurcations will be designated β_{nfmb}. For specificity, our calculations were performed for a particular bifurcation mechanism from the set that generates a B-type splitting, namely $(34)^*$. The possibilities that we have considered in the present work are listed in Table VII, along with the corresponding permutation–inversion (PI) generators. Our conclusions would not be qualitatively different if we had chosen $(12)^*$ or $(56)^*$ as the bifurcation generator. One further simplification is made, namely, we do not distinguish between matrix elements with different numbers of primes, such as β_{1f1b} and β'_{1f1b}; these matrix elements are not equivalent by symmetry, but we expect them to be similar because they involve the same number of flip and bifurcation paths.

The most general splitting pattern is given in Table VIII. The generators corresponding to β_{1f1b} and β'_{1f1b} each result in the A pattern when combined on their own with the single flip, if the corresponding matrix elements are small in magnitude compared to β_{1f}, in agreement with previous work.[7,10] Similarly, the generators for the alternative bifurcation paths, $(12)^*$ and $(56)^*$, give the B pattern if they are combined on their own with the generator for the single flip in the appropriate limit. However, it is important to realize that once a generator for the bifurcation has been chosen, the alternative choices no longer correspond to an elementary bifurcation, but to a bifurcation in combination with additional flips.

IV. THE $(D_2O)_3$ HIGH BARRIER LIMIT

Here we consider the limit $|\beta_{1b}| \ll |\beta_{1f}|$ and first confirm that the experimentally observed splitting pattern corresponds to case B.[10] Including the alternative multiple rearrangement pathways listed in Table VII we then express the β_i parameters of all the torsional states as a function of the value in the ground state, $\beta_i(0^0) \equiv \beta_i^0$, using the experimental values for the regular quartets and Tables VI and IX. Finally, we "tune" the β_i^0 to fit the matrix elements in all the torsional states, using the experimental values for the anomalous quartets and Tables VI and IX. The seven experimentally observed intermolecular VRT bands of $(D_2O)_3$ are listed in Table IV. If bifurcation splitting is entirely ne-

TABLE VIII. Splitting patterns for water trimer when certain other pathways are also allowed to contribute nonzero matrix elements. We assume that matrix elements for pathways involving the same number of elementary flip and bifurcation process are the same, e.g., $\beta_{1f1b}=\beta'_{1f1b}$.

$k=0$		
1	$2\beta_{1f}+2\beta_{2f}+\beta_{3f}+\beta_{1b}+4\beta_{1f1b}+6\beta_{2f1b}$	A_1^+
2	$\frac{1}{2}(\beta_{1f}+\beta_{2f}+2\beta_{3f}+2\beta_{1f1b}+4\beta_{2f1b}+\sqrt{9(\beta_{1f}^2+\beta_{2f}^2)+4(\beta_{1b}+\beta_{1f1b})(\beta_{1f}+\beta_{2f}+\beta_{1b}+\beta_{1f1b})+18\beta_{1f}\beta_{2f}})$	T_1^+
3	$\frac{1}{2}(\beta_{1f}+\beta_{2f}+2\beta_{3f}-2\beta_{1f1b}-4\beta_{2f1b}+\sqrt{9(\beta_{1f}^2+\beta_{2f}^2)-4(\beta_{1b}+\beta_{1f1b})(\beta_{1f}+\beta_{2f}-\beta_{1b}-\beta_{1f1b})+18\beta_{1f}\beta_{2f}})$	T_2^+
4	$2\beta_{1f}+2\beta_{2f}+\beta_{3f}-\beta_{1b}-4\beta_{1f1b}-6\beta_{2f1b}$	A_2^+
$k=\pm1$		
5	$\beta_{1f}-\beta_{2f}-\beta_{3f}+\beta_{1b}+2\beta_{1f1b}$	E_1^-
6	$\beta_{1f}-\beta_{2f}-\beta_{3f}+\beta_{1b}+2\beta_{1f1b}-2\beta_{2f1b}$	T_2^-
7	$\frac{1}{2}(-\beta_{1f}+\beta_{2f}-2\beta_{3f}+2\beta_{1f1b}-4\beta_{2f1b}+\sqrt{9(\beta_{1f}^2+\beta_{2f}^2)+4(\beta_{1b}-\beta_{1f1b})(\beta_{1f}-\beta_{2f}+\beta_{1b}-\beta_{1f1b})-18\beta_{1f}\beta_{2f}})$	T_1^-
8	$\frac{1}{2}(-\beta_{1f}+\beta_{2f}-2\beta_{3f}-2\beta_{1f1b}+4\beta_{2f1b}+\sqrt{9(\beta_{1f}^2+\beta_{2f}^2)+4(\beta_{1b}-\beta_{1f1b})(\beta_{2f}-\beta_{1f}+\beta_{1b}-\beta_{1f1b})-18\beta_{1f}\beta_{2f}})$	T_2^-
9	$\beta_{1f}-\beta_{2f}-\beta_{3f}-\beta_{1b}-2\beta_{1f1b}+2\beta_{2f1b}$	T_1^-
10	$\beta_{1f}-\beta_{2f}-\beta_{3f}-\beta_{1b}-2\beta_{1f1b}$	E_2^-
$k=\pm2$		
11	$-\beta_{1f}-\beta_{2f}+\beta_{3f}+\beta_{1b}-2\beta_{1f1b}$	E_2^+
12	$-\beta_{1f}-\beta_{2f}+\beta_{3f}+\beta_{1b}-2\beta_{1f1b}-2\beta_{2f1b}$	T_1^+
13	$\frac{1}{2}(\beta_{1f}+\beta_{2f}+2\beta_{3f}-2\beta_{1f1b}-4\beta_{2f1b}-\sqrt{9(\beta_{1f}^2+\beta_{2f}^2)-4(\beta_{1b}+\beta_{1f1b})(\beta_{1f}+\beta_{2f}-\beta_{1b}-\beta_{1f1b})+18\beta_{1f}\beta_{2f}})$	T_2^+
14	$\frac{1}{2}(\beta_{1f}+\beta_{2f}+2\beta_{3f}+2\beta_{1f1b}+4\beta_{2f1b}-\sqrt{9(\beta_{1f}^2+\beta_{2f}^2)+4(\beta_{1b}+\beta_{1f1b})(\beta_{1f}+\beta_{2f}+\beta_{1b}+\beta_{1f1b})+18\beta_{1f}\beta_{2f}})$	T_1^+
15	$-\beta_{1f}-\beta_{2f}+\beta_{3f}-\beta_{1b}+2\beta_{1f1b}+2\beta_{2f1b}$	T_2^+
16	$-\beta_{1f}-\beta_{2f}+\beta_{3f}-\beta_{1b}+2\beta_{1f1b}$	E_1^+
$k=3$		
17	$-2\beta_{1f}+2\beta_{2f}-\beta_{3f}+\beta_{1b}-4\beta_{1f1b}+6\beta_{2f1b}$	A_2^-
18	$\frac{1}{2}(-\beta_{1f}+\beta_{2f}-2\beta_{3f}-2\beta_{1f1b}+4\beta_{2f1b}-\sqrt{9(\beta_{1f}^2+\beta_{2f}^2)+4(\beta_{1b}-\beta_{1f1b})(\beta_{2f}-\beta_{1f}+\beta_{1b}-\beta_{1f1b})-18\beta_{1f}\beta_{2f}})$	T_2^-
19	$\frac{1}{2}(-\beta_{1f}+\beta_{2f}-2\beta_{3f}+2\beta_{1f1b}-4\beta_{2f1b}-\sqrt{9(\beta_{1f}^2+9\beta_{2f}^2)+4(\beta_{1b}-\beta_{1f1b})(\beta_{1f}-\beta_{2f}+\beta_{1b}-\beta_{1f1b})-18\beta_{1f}\beta_{2f}})$	T_1^-
20	$-2\beta_{1f}+2\beta_{2f}-\beta_{3f}-\beta_{1b}+4\beta_{1f1b}-6\beta_{2f1b}$	A_1^-

glected, fitting the observed torsional band origins provides us with values for the matrix elements corresponding to single, double and triple flips, i.e., β_{1f}, β_{2f}, and β_{3f}. The energy levels are perturbed from the single flip case that is isomorphic to the Hückel π system in benzene [Eq. (1)],[7] but the degeneracies are uneffected. The results are shown in Table X for $(D_2O)_3$ and Table XI for $(H_2O)_3$, and suggest that the single flip itself accounts for most of the observed splitting, with double and triple flips contributing only about 7% and 3% in $(D_2O)_3$ and 1% each in $(H_2O)_3$, respectively.

As the torsional motion is nearly barrierless, we have considered tunneling matrix elements corresponding to elementary bifurcation accompanied by additional torsional flips. All the bifurcation tunneling splittings observed for $(D_2O)_3$ are very small (<10 MHz), so that the $|\beta_{1b}| \ll |\beta_{1f}|$ limit should still be valid. We have therefore restricted our analysis to matrix elements corresponding to single bifurcations accompanied by up to two flips (Table IX).

From the regular quartets it is not possible to distinguish between the A and B splitting patterns if the matrix elements vary within each torsional manifold. However, for both patterns, it is possible to calculate effective β_b's for all the torsional energy levels as a function of the corresponding parameter in the $k=0^\circ$ state, $\beta_b^0 \equiv \beta_b(0^0)$, using the regular quartets and Table VI. (A definition of β_b for the B pattern is given below.) The ''anomalous'' quartets observed in $K=0$ states allow us to distinguish between the two patterns and to estimate β_b^0.

From such an analysis of the anomalous quartets of the 98 cm^{-1} band, Olthof *et al.* concluded that the bifurcation tunneling pathway corresponds to the B pattern, rather than the A.[35] If β_b is not fixed within each torsional manifold, a

TABLE IX. Splitting patterns for water trimer when the pathways listed in Table VII contribute nonzero matrix elements. Here we consider the limit where both $|\beta_{1b}|$ and $|\beta_{1f1b}|$ are small.

$k=0$		
1	$2\beta_{1f}+2\beta_{2f}+\beta_{3f}+\beta_{1b}+4\beta_{1f1b}+6\beta_{2f1b}$	A_1^+
2	$2\beta_{1f}+2\beta_{2f}+\beta_{3f}+\frac{1}{3}\beta_{1b}+\frac{4}{3}\beta_{1f1b}+2\beta_{2f1b}$	T_1^+
3	$2\beta_{1f}+2\beta_{2f}+\beta_{3f}-\frac{1}{3}\beta_{1b}-\frac{4}{3}\beta_{1f1b}-2\beta_{2f1b}$	T_2^+
4	$2\beta_{1f}+2\beta_{2f}+\beta_{3f}-\beta_{1b}-4\beta_{1f1b}-6\beta_{2f1b}$	A_2^+
$k=\pm1$		
5	$\beta_{1f}-\beta_{2f}-\beta_{3f}+\beta_{1b}+2\beta_{1f1b}$	E_1^-
6	$\beta_{1f}-\beta_{2f}-\beta_{3f}+\beta_{1b}+2\beta_{1f1b}-2\beta_{2f1b}$	T_2^-
7	$\beta_{1f}-\beta_{2f}-\beta_{3f}+\frac{1}{3}\beta_{1b}+\frac{2}{3}\beta_{1f1b}-2\beta_{2f1b}$	T_1^-
8	$\beta_{1f}-\beta_{2f}-\beta_{3f}-\frac{1}{3}\beta_{1b}-\frac{2}{3}\beta_{1f1b}+2\beta_{2f1b}$	T_2^-
9	$\beta_{1f}-\beta_{2f}-\beta_{3f}-\beta_{1b}-2\beta_{1f1b}+2\beta_{2f1b}$	T_1^-
10	$\beta_{1f}-\beta_{2f}-\beta_{3f}-\beta_{1b}-2\beta_{1f1b}$	E_2^-
$k=\pm2$		
11	$-\beta_{1f}-\beta_{2f}+\beta_{3f}+\beta_{1b}-2\beta_{1f1b}$	E_2^+
12	$-\beta_{1f}-\beta_{2f}+\beta_{3f}+\beta_{1b}-2\beta_{1f1b}-2\beta_{2f1b}$	T_1^+
13	$-\beta_{1f}-\beta_{2f}+\beta_{3f}+\frac{1}{3}\beta_{1b}-\frac{2}{3}\beta_{1f1b}-2\beta_{2f1b}$	T_2^+
14	$-\beta_{1f}-\beta_{2f}+\beta_{3f}-\frac{1}{3}\beta_{1b}+\frac{2}{3}\beta_{1f1b}+2\beta_{2f1b}$	T_1^+
15	$-\beta_{1f}-\beta_{2f}+\beta_{3f}-\beta_{1b}+2\beta_{1f1b}+2\beta_{2f1b}$	T_2^+
16	$-\beta_{1f}-\beta_{2f}+\beta_{3f}-\beta_{1b}-2\beta_{1f1b}$	E_1^+
$k=3$		
17	$-2\beta_{1f}+2\beta_{2f}-\beta_{3f}+\beta_{1b}-4\beta_{1f1b}+6\beta_{2f1b}$	A_2^-
18	$-2\beta_{1f}+2\beta_{2f}-\beta_{3f}+\frac{1}{3}\beta_{1b}-\frac{4}{3}\beta_{1f1b}+2\beta_{2f1b}$	T_2^-
19	$-2\beta_{1f}+2\beta_{2f}-\beta_{3f}-\frac{1}{3}\beta_{1b}+\frac{4}{3}\beta_{1f1b}-2\beta_{2f1b}$	T_1^-
20	$-2\beta_{1f}+2\beta_{2f}-\beta_{3f}-\beta_{1b}+4\beta_{1f1b}-6\beta_{2f1b}$	A_1^-

value of β_b^0 can be found for both patterns that fits the anomalous quartets observed in the 98 cm^{-1} band, as well as all the regular quartets. However, only the B splitting pattern can also explain the observed anomalous splittings of the 28 cm^{-1} band. We therefore conclude that in $(D_2O)_3$ the bifurcation tunneling pathway indeed corresponds to the B pattern. From Table VII it follows that bifurcation tunneling proceeds via a pathway corresponding to one of the generators (12)*, (34)*, or (56)*. It is worth noting that some of the pathways corresponding to the generators for β_{1f1b} and β_{2f1b} result in the A pattern, when combined individually

TABLE X. Fitted matrix elements for $(D_2O)_3$. The three torsional matrix elements corresponding to single, double, and triple flips could all be fitted for $k=n^0$, but for $k=n^1$ only β_{1f} could be estimated because only two levels have been observed. The values of the effective tunneling matrix elements, β_b, as a function of $\beta_b(0^0)\equiv\beta_b^0$ calculated from the regular tunneling splittings are shown, as well as the absolute value of β_b associated with the dominant pathway determined by the analysis of the anomalous $K=0$ quartets of the 98 and 28 cm^{-1} bands. The effective matrix elements are defined in the text. The last column shows the effective matrix elements with the value of $\beta_b(0^0)$ determined from the anomalous quartets. The parameters β_{1f}, β_{2f}, and β_{3f} are reported in cm^{-1}, but all the other matrix elements are in MHz.

k	β_{1f}	β_{2f}	β_{3f}	β_b	β_b
0^0				β_b^0	~-0.55
$\pm1^0$	-10.08	0.75	-0.33	$-0.9-\beta_b^0$	~-0.35
$\pm2^0$				$1.35+\beta_b^0$	~0.8
3^0				$-2.25-\beta_b^0$	~-1.7
3^1				$3.15-\beta_b^0$	~3.7
	8.8				
$\pm2^1$				$-7.5+\beta_b^0$	~-8.05

TABLE XI. Fitted torsional and bifurcation matrix elements (MHz) for $(H_2O)_3$ for the limit $|\beta_{1b}|\ll|\beta_{1f}|$. These values of the effective tunneling matrix elements β_b as a function of $\beta_b(0^0)\equiv\beta_b^0$, calculated from the regular tunneling splittings, are about a hundred times larger than for $(D_2O)_3$. The effective matrix elements have the same definition as in $(D_2O)_3$. $\beta_{1f}=-21.67$, $\beta_{2f}=-0.20$, and $\beta_{3f}=-0.22$ cm^{-1}.

k	β_b
0^0	β_b^0
$\pm1^0$	$-441-\beta_b^0$
$\pm2^0$	$382.5+\beta_b^0$
3^0	$-433.5-\beta_b^0$

with the single flip. However, once (34)* is chosen as the elementary bifurcation these other generators correspond to elementary bifurcations with additional flips. In order to quantify the magnitude of the bifurcation matrix elements in the different torsional states, we use the energy expressions in Table IX. Even though we have chosen (34)* as the elementary bifurcation, and thus expect the matrix elements β_{1b} to be larger than β_{1f1b} or β_{2f1b}, it is not possible to distinguish the different contributions to the regular quartets. From the regular quartets it is only possible to evaluate an effective β_b, which is a combination of β_{1b}, β_{1f1b} and β_{2f1b} for the different torsional levels, as a function of β_b^0. The results are shown in Table X, and the effective β_b for all torsional states are:

$$\beta_b(0^0)=\beta_{1b}(0^0)+4\beta_{1f1b}(0^0)+6\beta_{2f1b}(0^0) \quad \text{for } k=0^0;$$

$$\beta_b(1^0)=\beta_{1b}(1^0)+2\beta_{1f1b}(1^0) \quad \text{for } k=\pm1^0;$$

$$\beta_b(2^n)=\beta_{1b}(2^n)-2\beta_{1f1b}(2^n) \quad \text{for } k=\pm2^n;$$

$$\beta_b(3^n)=\beta_{1b}(3^n)-4\beta_{1f1b}(3^n)+6\beta_{2f1b}(3^n) \quad \text{for } k=3^n.$$

The magnitude of β_b^0 was next adjusted to reproduce both the anomalous quartets of the 28 cm^{-1} and 98 cm^{-1} bands, thus quantifying the magnitude of the tunneling splittings and the effective β_b for all the torsional states (see Table X). The values determined for $\beta_b(1^0)$ and $\beta_b(2^0)$ also produce a small J-independent "asymmetric" doublet splitting for $K=0$ transitions of the 19.5 cm^{-1} band, which was indeed observed experimentally. Each doublet transition consists of a convolution of three transitions, and our results predict the higher frequency transition to be slightly broader and more intense, in detailed agreement with the experiment. We note that the adjusted fitted values are consistent with our original assumption that $|\beta_{1b}|\ll|\beta_{1f}|$ and quantitatively reproduce both the regular and anomalous bifurcation tunneling patterns in all the torsional transitions. Finally, we note that we have not included the 142.8 cm^{-1} band. The anomalous splitting of $K=0$ in this band has been described before but not fully explained.[24]

V. BREAKDOWN OF THE HIGH BARRIER LIMIT IN $(H_2O)_3$

The effect of increasing energy in the bifurcation tunneling coordinate was not considered in previous studies, as only a limited dataset was available. The detailed analysis of the torsional $(H_2O)_3$ bands by Brown *et al.* revealed some unexplained shifts of the *T* states with respect to the *A* states, including both *J*- and *K*-dependent and independent components.[23] Keutsch *et al.* reported at least three widely spaced subbands of the 520 cm^{-1} librational band, which similarly preclude an equally spaced quartet.[25]

There is less experimental information available for $(H_2O)_3$ than for $(D_2O)_3$. Hence it is not possible to distinguish between the *A* and *B* patterns, as no information on ''anomalous'' quartets is yet available. This lack of data also precludes a quantitative determination of β_b^0 and thus of all the other matrix elements. In the following analysis we assume that the *B* pattern is also dominant for $(H_2O)_3$. For the torsional states, we can only evaluate the effective matrix elements β_b as a function of β_b^0, as for $(D_2O)_3$. The results are shown in Table XI and an estimate of $\beta_b^0 = -200$ MHz results in bifurcation matrix elements that have similar absolute magnitudes for all torsional states, comparable to the more detailed results for $(D_2O)_3$. Unfortunately, we are not able to determine the origin of the shift observed by Brown *et al.*[23] We note that inclusion of multiple bifurcation events will result in such a shift. However, pathways corresponding to more than one bifurcation rearrangement are not expected to contribute significantly because the $|\beta_{1b}| \ll |\beta_{1f}|$ limit still applies quite well to these states. This conclusion follows both from the fact that for the near barrierless flip, such multiple tunneling events are nearly negligible, and from the results for the librational band below.

The analysis of Olthof *et al.* showed that the *J*-dependent splitting of the $K = \pm 1$ states of the $k = 0^0$ and 3^0 levels can only be explained if the bifurcation tunneling parameters in these levels, $\delta(0^1) = 2(\beta_2 - \beta_3)/3$ and $\delta(0^2) = 2(2\beta_2 + \beta_3)/3$, have opposite signs. Here β_2 and β_3 correspond to the generators (ACB)(164253) and (34)*; β_3 is one component of our β_b, while β_2 would generate the *A* pattern if combined on its own with the single flip. If we assume that the *B* pattern is dominant and β_2 is negligible, then our results (see Table XI) only allow a choice of opposite signs with $\beta_b(0^0) < -433.5$ MHz, resulting in a much smaller magnitude for β_b in the $k = 1^0$ and $k = 2^0$ states. This assignment seems unlikely, and suggests that other generators that contribute to our effective β_b may also be involved in the *J*-dependent splitting of the $K = \pm 1$ states for $k = 0^0$ and 3^0.

For the librational band, the analysis is more difficult, as only three of the four tunneling components have been observed and their symmetries could not be determined. In this band the bifurcation splitting is so large that each of the four components appears as an individual subband, rather than as one rotational transition split by bifurcation tunneling into a quartet. It is, however, clear that the subband corresponding to the A_1 symmetry state was not observed, because it only has nonzero intensity for $K = 3m$ and therefore should be easily identifiable, as only every third transition is observed in each *P* and *R* branch. The three subbands are centered at 517.2, 523.9, and 525.3 cm^{-1}. The 523.9 cm^{-1} band is probably a *T* state, since it has a *J*-dependent splitting of the $K = 1$ levels analogous to that of the *T* states of the 87 cm^{-1} band. The splitting was observed in the *P*, *Q*, and *R* branches of the 523.9 cm^{-1} band, whereas it was only observed in the *P* and *R* branches in the 87 cm^{-1} band. This result is understandable if the observed splitting is dominated by the upper state contribution in the librational bands, whereas in the 87 cm^{-1} band it arises instead from the sum of the splittings in the upper and lower levels in the *P* and *R* branches and the difference of the splittings in the *Q* branch. The $K = 1$ splitting of the 523.9 cm^{-1} band is about three orders of magnitude larger than in the 87 cm^{-1} band, providing strong evidence that the bifurcation matrix elements are much larger in the librational state. It is not possible to make a quantitative estimate, as the splitting depends on the Coriolis coupling to the nearest degenerate states, which is not known. It is unclear why no $|K| = 1$ splitting of either of the other two assigned subbands was observed, even though one of them is thought to be a *T* state.

Although no detailed assignment of tunneling symmetries is possible for the observed librational band at present, an estimate of the magnitude of the bifurcation tunneling splitting may be obtained from the smallest observed splitting, (1.4 cm^{-1} or about 42 000 MHz), which is some three orders of magnitude larger than in the torsional states. It is therefore clear that the bifurcation splitting in the excited state of the 520 cm^{-1} band is many orders of magnitude larger than in the ground state. The limit $|\beta_{1b}| \ll |\beta_{1f}|$ is no longer valid and the more general results from Table III have to be used. We assume that the three bands correspond to the A_2, T_1, and T_2 components, which results in six possible assignments. The two assignments with the A_2 symmetry corresponding to the 523.9 cm^{-1} band are unlikely because of the splitting of the $K = 1$ states. The symmetry of the observed excited vibrational state is A_1^- and the transition corresponds to excitation of the A_1^- out-of-plane libration.[25] The splittings from torsion and bifurcation therefore follow the energy expression for the ground state, with the exception that the general expression (center column) in Table III has to be used. Interestingly, the only assignments that results in real matrix elements is if the symmetry of the 525.3 cm^{-1} subband is T_1^-, the 523.9 cm^{-1} subband T_2^-, and the 517.2 cm^{-1} subband A_2^-. The values of the bifurcation and torsional matrix elements are either $\beta_{1f} = -3.1$ cm^{-1} and $\beta_{1b} = -2.3$ cm^{-1}, or $\beta_{1f} = 1.6$ cm^{-1} and $\beta_{1b} = 4.6$ cm^{-1}. This shows that for both assignments $|\beta_{1b}| \ll |\beta_{1f}|$ is indeed no longer valid.

It is also possible that pathways corresponding to more than one bifurcation could contribute to tunneling for this band. However, we have already noted that the effect of double and triple flip paths is small compared to the single flip mechanism, so this explanation is probably less likely.

VI. CONCLUSIONS

We have presented fits of the observed terahertz VRT spectra of $(H_2O)_3$ and $(D_2O)_3$ for transitions that correspond

to excitation of torsional and librational states. For $(D_2O)_3$, the transitions are fitted for the limit $|\beta_{1b}| \ll |\beta_{1f}|$ using matrix elements corresponding to single, double, and triple flips, the elementary bifurcation path, and a path corresponding to bifurcation plus an extra flip. Aside from the purely torsional matrix elements, the fit provides tunneling parameters for the excited states in terms of the value of the corresponding parameter in the $k=0^0$ state. In agreement with the analysis of Olthof *et al.*, we find that the bifurcation pathway corresponds to the *B* splitting pattern,[7,10] where bifurcation is accompanied by two simultaneous flips. The corresponding permutation–inversion generator is one of (12)*, (34)*, or (56)*.

A quantitative fit of the effective bifurcation matrix elements for $(D_2O)_3$ was made possible by the analysis of all the regular splittings of all the observed bands along with the anomalous splittings of the 28 and 98 cm^{-1} bands. We currently have no definitive explanation for the anomalous splittings of the 142.8 cm^{-1} band, which remains the only unexplained spectral feature for any observed $(D_2O)_3$ VRT band.

The analysis of the bifurcation tunneling dynamics in $(H_2O)_3$ does not allow such a quantitative description, however we can express the effective bifurcation matrix elements in terms of the corresponding parameters for $k=0^0$, which we estimate to be around -200 MHz. We can also explain the splitting of the $K=1$ states in the 523.9 cm^{-1} band and suggest that the splittings in the librational band do not require the involvement of tunneling pathways containing multiple flips or bifurcations, but instead reflect the breakdown of the $|\beta_{1b}| \ll |\beta_{1f}|$ limit. However, we cannot determine how much tunneling pathways with additional flips might contribute to the overall tunneling splitting. More experimental work is necessary to determine all the tunneling components of the librational band, and possible degenerate vibrational states in the vicinity, to evaluate the Coriolis parameter for the $K=1$ splitting of the 523.9 cm^{-1} band and to identify the subband corresponding to the A_1 tunneling symmetry.

ACKNOWLEDGMENTS

The authors wish to thank Mac G. Brown for many helpful discussions. This work was supported by the Experimental Physical Chemistry Program of the National Science Foundation.

[1] F. N. Keutsch and R. J. Saykally, Proc. Natl. Acad. Sci. U.S.A. **98**, 10533 (2001).
[2] R. S. Fellers, C. Leforestier, L. B. Braly, M. G. Brown, and R. J. Saykally, Science **284**, 945 (1999).
[3] C. Leforestier, L. B. Braly, K. Liu, M. J. Elrod, and R. J. Saykally, J. Chem. Phys. **106**, 8527 (1997).
[4] G. C. Groenenboom, P. E. S. Wormer, A. van der Avoird, E. M. Mas, R. Bukowski, and K. Szalewicz, J. Chem. Phys. **113**, 6702 (2000).
[5] G. C. Groenenboom, E. M. Mas, R. Bukowski, K. Szalewicz, P. E. S. Wormer, and A. van der Avoird, Phys. Rev. Lett. **84**, 4072 (2000).
[6] E. M. Mas, R. Bukowski, K. Szalewicz, G. C. Groenenboom, P. E. S. Wormer, and A. van der Avoird, J. Chem. Phys. **113**, 6687 (2000).
[7] D. J. Wales, J. Am. Chem. Soc. **115**, 11180 (1993).
[8] D. J. Wales and T. R. Walsh, J. Chem. Phys. **105**, 6957 (1996).
[9] D. J. Wales and T. R. Walsh, J. Chem. Phys. **106**, 7193 (1997).
[10] T. R. Walsh and D. J. Wales, J. Chem. Soc., Faraday Trans. **92**, 2505 (1996).
[11] A. van der Avoird, E. H. T. Olthof, and P. E. S. Wormer, J. Chem. Phys. **105**, 8034 (1996).
[12] K. Liu, J. G. Loeser, M. J. Elrod, B. C. Host, J. A. Rzepiela, N. Pugliano, and R. J. Saykally, J. Am. Chem. Soc. **116**, 3507 (1994).
[13] K. Liu, M. G. Brown, J. D. Cruzan, and R. J. Saykally, Science **271**, 62 (1996).
[14] F. N. Keutsch, R. S. Fellers, M. G. Brown, V. M. R., P. B. Petersen, and R. J. Saykally, J. Am. Chem. Soc. **123**, 5938 (2001).
[15] J. K. Gregory and D. C. Clary, J. Chem. Phys. **105**, 6626 (1996).
[16] J. K. Gregory and D. C. Clary, J. Chem. Phys. **102**, 7817 (1995).
[17] M. G. Brown, F. N. Keutsch, L. B. Braly, and R. J. Saykally, J. Chem. Phys. **111**, 7801 (1999).
[18] M. G. Brown, F. N. Keutsch, and R. J. Saykally, J. Chem. Phys. **109**, 9645 (1998).
[19] L. B. Braly, J. D. Cruzan, K. Liu, R. S. Fellers, and R. J. Saykally, J. Chem. Phys. **112**, 10293 (2000).
[20] L. B. Braly, K. Liu, M. G. Brown, F. N. Keutsch, R. S. Fellers, and R. J. Saykally, J. Chem. Phys. **112**, 10314 (2000).
[21] M. R. Viant, J. D. Cruzan, D. D. Lucas, M. G. Brown, K. Liu, and R. J. Saykally, J. Phys. Chem. A **101**, 9032 (1997).
[22] M. R. Viant, M. G. Brown, J. D. Cruzan, R. J. Saykally, M. Geleijns, and A. van der Avoird, J. Chem. Phys. **110**, 4369 (1999).
[23] M. G. Brown, M. R. Viant, R. P. McLaughlin, C. J. Keoshian, E. Michael, J. D. Cruzan, R. J. Saykally, and A. van der Avoird, J. Chem. Phys. **111**, 7789 (1999).
[24] F. N. Keutsch, M. G. Brown, P. B. Petersen, R. J. Saykally, M. Geleijins, and A. van der Avoird, J. Chem. Phys. **114**, 3994 (2001).
[25] F. N. Keutsch, R. S. Fellers, M. R. Viant, and R. J. Saykally, J. Chem. Phys. **114**, 4005 (2001).
[26] F. N. Keutsch, E. N. Karyakin, R. J. Saykally, and A. van der Avoird, J. Chem. Phys. **114**, 3988 (2001).
[27] J. D. Cruzan, M. R. Viant, M. G. Brown, and R. J. Saykally, J. Phys. Chem. A **101**, 9022 (1997).
[28] K. Liu, M. G. Brown, C. Carter, R. J. Saykally, J. K. Gregory, and D. C. Clary, Nature (London) **381**, 501 (1996).
[29] D. Sabo, Z. Bačić, T. Bürgi, and S. Leutwyler, Chem. Phys. Lett. **244**, 283 (1995).
[30] W. Klopper and M. Schütz, Chem. Phys. Lett. **237**, 536 (1995).
[31] D. Sabo, Z. Bačić, T. Bürgi, and S. Leutwyler, Chem. Phys. Lett. **261**, 318 (1996).
[32] D. Sabo, Z. Bačić, S. Graf, and S. Leutwyler, J. Chem. Phys. **110**, 5745 (1999).
[33] D. Sabo, Z. Bačić, S. Graf, and S. Leutwyler, J. Chem. Phys. **111**, 5331 (1999).
[34] D. Sabo, Z. Bačić, S. Graf, and S. Leutwyler, J. Chem. Phys. **111**, 10727 (1999).
[35] E. H. T. Olthof, A. van der Avoird, P. E. S. Wormer, K. Liu, and R. J. Saykally, J. Chem. Phys. **105**, 8051 (1996).
[36] J. C. Owicki, L. L. Shipman, and H. A. Scheraga, J. Phys. Chem. **79**, 1794 (1975).
[37] J. E. Fowler and H. F. Schaefer, J. Am. Chem. Soc. **117**, 446 (1995).
[38] H. C. Longuet-Higgins, Mol. Phys. **6**, 445 (1963).
[39] T. Bürgi, S. Graf, S. Leutwyler, and W. Klopper, J. Chem. Phys. **103**, 1077 (1995).
[40] P. R. Bunker and P. Jensen, *Molecular Symmetry and Spectroscopy*, 2nd ed. (NRC Research, Ottawa, 1998).
[41] N. Pugliano and R. J. Saykally, Science **257**, 1937 (1992).
[42] R. G. A. Bone, T. W. Rowlands, N. C. Handy, and A. J. Stone, Mol. Phys. **72**, 33 (1991).
[43] T. Taketsugu and D. J. Wales, Mol. Phys. **100**, 2793 (2002).
[44] R. E. Leone and P. v. R. Schleyer, Angew. Chem. Int. Ed. Engl. **9**, 860 (1970).
[45] D. Sabo, Z. Bačić, S. Graf, and S. Leutwyler, J. Chem. Phys. **109**, 5404 (1998).
[46] D. J. Wales, in *Theory of Atomic and Molecular Clusters*, edited by J. Jellinek (Springer-Verlag, Heidelberg, 1999), pp. 86–110.
[47] J. K. Gregory and D. C. Clary, J. Phys. Chem. **100**, 18014 (1996).
[48] J. K. Gregory, D. C. Clary, K. Liu, M. G. Brown, and R. J. Saykally, Science **275**, 814 (1997).
[49] J. K. Gregory and D. C. Clary, in *Advances in Molecular Vibrations and Collision Dynamics*, edited by J. M. Bowman and Z. Bačić (JAI, Stamford, 1998), Vol. 3, pp. 311–359.
[50] V. Buch, P. Sandler, and J. Sadlej, J. Phys. Chem. B **102**, 8641 (1998).

[51] E. Fredj, R. B. Gerber, and M. A. Ratner, J. Chem. Phys. **105**, 1121 (1996).
[52] J. O. Jung and R. B. Gerber, J. Chem. Phys. **105**, 10332 (1996).
[53] P. R. Bunker, J. Mol. Spectrosc. **176**, 297 (1996).
[54] M. Kolbuszewski and P. R. Bunker, J. Chem. Phys. **105**, 3649 (1996).
[55] S. Suzuki and G. A. Blake, Chem. Phys. Lett. **229**, 499 (1994).
[56] K. Liu, M. J. Elrod, J. G. Loeser, J. D. Cruzan, N. Pugliano, M. G. Brown, J. Rzepiela, and R. J. Saykally, Faraday Discuss. **97**, 35 (1994).